Evaluating Spatiotemporal Patterns and Trends of Drought in Japan Associated with Global Climatic Drivers

Ke Shi[1], Yoshiya Touge[1], So Kazama[1]

[1] Department of Civil and Environmental Engineering, Tohoku University, Aramakiaza Aoba 6-6-06, Aoba, Sendai, Miyagi, 980-8579, Japan

Correspondence: Ke Shi (ke.dlut@outlook.com)

Abstract: Drought disasters, such as water scarcity and wildfires, are serious natural disasters in Japan that are also affected by climate change. However, as drought generally has widespread impacts and the duration of drought can vary considerably, it is difficult to assess the spatiotemporal characteristics and the climatic causes of drought. Therefore, to identify the drought homogeneous regions and understand climatic causes of regional drought over Japan, this study provides a spatiotemporal analysis for historical droughts patterns and teleconnections associated with global climatic drivers. The trends of meteorological elements, which are the basis of drought index calculation, was first assessed. Then, drought characterized by the Self-calibrating Palmer Drought Severity Index (scPDSI) was investigated. Trends and patterns of drought were identified through the trend-free pre-whitening Mann-Kendall test and distinct empirical orthogonal function. The continuous wavelet transform and cross wavelet transform together with wavelet coherence were utilized to depict the links between drought and global climatic drivers. The results are described as follows: (1) the trends of precipitation were insignificant. However, temperature and potential evapotranspiration increasing trends were detected over Japan; (2) the drought trend over Japan varied seasonally, increasing in spring and summer and decreasing in autumn and winter; (3) two major subregions of drought variability—the western Japan (W region) and most of the northernmost Japan near the Pacific (N region) were identified; (4) wildfires with large burned area were more likely to occur when the scPDSI was less than -1; and (5) the North Atlantic Index (NAOI) showed the strongest coherence connections with Distinguished Principle Components-1 among four

28   climatic drivers. Additionally, Distinguished Principle Components-2 showed stronger coherence

29   connections with NAOI and Arctic Oscillation Index. This study is the first to identify homogeneous

30   regions with distinct drought characteristics over Japan and connect the drought in Japan with the

31   global climatic drivers.

32   **Key Words:** Drought; scPDSI; DEOF; Spatiotemporal patterns; Wavelet analysis; Climatic causes.

1. Introduction

34   Under climate change conditions, especially direct and clear global warming (IPCC, 2014),

35   drought has shown increasing trends in certain regions of the world (Cook et al., 2004; Dai, 2011,

36   2013; Kogan and Guo, 2016). Contrasted with permanent aridity in arid areas, drought is a

37   temporary reduction in precipitation or water availability over an extended period (Hisdal, 2000) and

38   can last for months or years. Considering the duration, intensity, geographical extent, and broad

39   effects of droughts, it is difficult to determine drought occurrences and their effects (Asong et al.,

40   2018). Additionally, drought is considered to be the most complex and impenetrable extreme climate

41   event, affecting more people than any other natural hazard (Hagman, 1984). Droughts can have

42   catastrophic impacts on the economy, society, and environment (Edwards et al., 2019; Wilhite et al.,

43   2007). For example, droughts experienced in Africa, Asia, Australia, South America, and Europe

44   have had devastating effects over large areas (Mishra and Singh, 2010). In particular, the deficit in

45   precipitation combined with high evapotranspiration losses during a drought would increase the risk

46   of other disasters such as wildfires (Sarris et al., 2014). The risk of water scarcity would be

47   exacerbated by long-term drought, which poses challenges to water resources management (Iglesias

48   et al., 2007).

49   The research on droughts over Japan has been receiving increasing attention. More than 70% of

50   Japan is mountainous, causing rain to flow quickly to the ocean after falling. Historically, most areas

51   of Japan have experienced droughts with varying duration, frequency, severity, and intensity.

52   Particularly, long-lasting droughts occurred over a large part of Japan in 1967, 1973, 1978, 1984,

53   1985, and 1994 (Okada, 2016). In 1994, almost the whole of Japan experienced a particularly

54   long-lasting drought and the drought caused an economic loss of approximately 1.3 billion dollars as

55   a result of the decline in agricultural production (Lee et al., 2012). The number of areas affected by

56   drought in Japan is decreasing but still exists every year (Okada, 2016). In 2007, due to the drought,

57   the leaf necrotic area percentage of sampled dogwood trees was significantly severe in Yamaguchi,

58   Japan (Wang et al., 2009). Also, due to climate change, the uncertainty of drought characterization in

59   Japan would bring more challenges to water management.

60   Indeed, drought is generally driven by multiple global climatic drivers, which are forced by

61   land-sea-atmosphere interactions (Sheffield et al., 2009). Therefore, to further understand the

62   drought characteristics and predict drought events, it is necessary to consider the relationship

63   between drought and global climate drivers (Asong et al., 2018). This type of research has been

64   carried out in different regions. Rajagopalan et al. (2000) selected the Palmer Drought Severity

65   Index (PDSI) to characterize drought and explored the impact of winter El Niño-Southern

66   Oscillation (ENSO) and global sea surface temperatures (SSTs) on summer drought in the United

67   States. Rangsiwanichpong et al. (2017) analysed the relationship between various ocean indices and

68   precipitation in the Chao Phraya River Basin. Actually, the decrease in precipitation is often a cause

69   of drought (Viste et al., 2013). Wang et al. (2015) explored the teleconnections of seven selected

70   climatic drivers with drought in the arid region of China. Asong et al. (2018) used the Standardized

71   Precipitation Evapotranspiration Index (SPEI) to identify drought patterns over Canada and analysed

72   their teleconnections with global climatic drivers. Their researches have contributed to

73   understanding the causes of drought across the region.

74   Considering that the drought over Japan has unique characteristics and may be different from

75   other global arid land. Similar research on the causes of drought over Japan also needs to be carried

76   out. The establishment of connection analysis between drought and global climatic drivers over

77   Japan will also help to understand the potential links between different regions of drought. For Japan,

78   choosing the appropriate global climatic drivers is first required. Previous studies have already

79   analysed the relationship between global climatic drivers and hydroclimate in Japan. He et al. (2017)

80   pointed out that the Arctic Oscillation (AO) affected freezing precipitation or snowfall events over

81   East Asia. A statistically significant positive relationship between the North Atlantic Oscillation

82   (NAO) and precipitation in the western region of Japan was also found (Aizen et al., 2001). Hu et al.

83   (2005) analysed the connection between the ENSO and East Asian precipitation variations, which

84   showed that an ENSO generates stronger precipitation anomalies than a non-ENSO. Lee et al. (2012)

85   pointed out that the Pacific Decadal Oscillation (PDO) has a certain impact on cyclone-induced

86   precipitation over East Asia. These global climatic drivers have already been confirmed to have

87   impacts on hydroclimate in Japan.

88   Overall, to further improve the capacity of early warning and risk assessment of drought at the

89   regional level, it is necessary to identify the homogeneous regions with distinct drought

90   characteristics over Japan and analyse the causes of drought. However, previous researches have

91   mainly focused on the phenomenon of drought events. There is still a lack of understanding of the

92   causes and specific consequences of the droughts in Japan. In other words, establishing the link

93   between nationwide drought properties in Japan and global climatic drivers has not been addressed

94   before. For this purpose, this study attempts to provide an in-depth analysis of historical droughts

95   over Japan to fill these gaps. The drought events were characterized by Self-calibrating Palmer

96   Drought Severity Index (scPDSI) using the most up-to-date data. Then trends in the meteorological

97   elements (precipitation, near-surface temperature, potential evapotranspiration) and scPDSI were

98   investigated by the trend-free pre-whitening Mann-Kendall (TFPW-MK) test. Major patterns of

99   long-term trends in drought and periodicity were then identified using the distinct empirical

100 orthogonal function (DEOF) and continuous wavelet transform, respectively. Additionally, the

101 relationship between drought index and wildfire was analysed to identify the effects of the drought.

102 Finally, the teleconnections between the major drought patterns and global climatic driving factors

103 were analysed by cross wavelet transform together with wavelet coherence.

104   This paper is organized as follows: Section 2 describes the data of the study area and analytical

105 methodology. In Section 3, the results and discussion are revealed. Finally, the summary and

106 conclusions are given in Section 4.

107 ## 2. Materials and Methodology

108 ### 2.1 Study area

109   The study area comprises the whole of Japan, which is an area mostly characterized by steep

110 mountainous terrain. Japan's total annual precipitation is approximately 1,719 mm, while the annual

111 precipitation per capita is approximately 5,100 m^3, which is only approximately 1/3 of the world

112   average of 16,800 m³ (MLIT, 2014). Moreover, water resources in Japan are significantly dependent

113   on the weather. Precipitation is generally concentrated in the rainy, typhoon, and snowfall seasons.

114   The country is so steep that most precipitation quickly runs off into the sea (Su et al., 2019).

115   **2.2 Data**

116   The 0.5° high-resolution gridded datasets of precipitation, near-surface temperature, potential

117   evapotranspiration, and scPDSI were obtained from the Climatic Research Unit (CRU) at the

118   University of East Anglia (Blunden et al., 2019; Harris et al., 2014; Van Der Schrier et al., 2013).The

119   period of scPDSI from CRU is currently from 1901 to 2018. Since this paper is mainly dedicated to

120   analysing the time trends and spatial homogeneity zone of drought, using data from the 1900s may

121   leading the trend of drought to be exaggerated. Besides, at an early stage, there was a problem of

122   sparse distribution of stations. Therefore, the time scale selected in this paper is from 1960 to 2018.

123   The scPDSI class is shown in Table 1 (Palmer, 1986). This scPDSI was presented by Wells et al.

124   (2004), which was a variant of the original PDSI (Palmer, 1986) used to make the results from

125   different climatic regimes more comparable. To better understand how scPDSI characterizes drought,

126   the main calculation formulas of scPDSI are listed as follows:

127   $$Z_i = K\left(P - \left(\alpha_i PE + \beta_i PR + \varphi_i PRO - \delta_i PL\right)\right) \tag{1}$$

128   The Z index can be used to show the dryness/wetness in month i. K is a climatic characteristic

129   value that varies over both time and space to account for climate changes. α_i, β_i, φ_i, and δ_i are the

130   weighted values according to the climate of the area. The P, PE, PR, PRO, and PL represent

131   precipitation, potential evapotranspiration, potential recharge, potential runoff, and potential loss,

132   respectively. Through the Z index, the scPDSI value can be calculated for a given month using the

133   following formula:

134   $$scPDSI_i = \eta scPDSI_{i-1} + \rho Z_i \tag{2}$$

135   where η and ρ represent the sensitivity of the index to precipitation events. For specific values, see

136   Van Der Schrier et al. (2013).

137   In particular, the potential evapotranspiration was calculated through the Penman-Monteith

138   equation rather than the Thornthwaite equation, which can more realistically estimate potential

139   evapotranspiration. The specific formula is listed as follows:

140
$$PET = \frac{0.408\Delta \, (R_n - G) + \gamma \frac{900}{T+273} U_2 \, (e_s - e_a)}{\Delta + \gamma \, (1 + 0.34 U_2)}$$
(3)

141   where R_n is the net radiation at the crop surface, G is the soil heat flux density, T is the air

142   temperature at the 2 m height, U_2 is the wind speed at the 2 m height, e_s is the vapour pressure of the

143   air at saturation, e_a is the actual vapour pressure, Δ is the slope of the vapour pressure curve and γ is

144   the psychrometric constant (Allen et al., 1998).

145   Additionally, scPDSI can deal with snow by adding a simple snowmelt and accumulation

146   process, which other drought indices, such as the Standardized Precipitation Index (SPI), Effective

147   Drought Index (EDI), and SPEI could not consider. Snowmelt was treated using the following

148   simple formula:

149
$$M = \beta T_{pdd}$$
(4)

150   where β is the degree-day factor and T_{pdd} is the sum of all positive daily mean temperatures during

151   the entire research period. For specific values, see Van Der Schrier et al. (2013)

152   The snow accumulation was estimated for each month from monthly mean temperature and

153   monthly precipitation as follows (Blunden et al., 2019; Harris et al., 2014; Van Der Schrier et al.,

154   2013):

155
$$f = \frac{1}{\sigma \sqrt{2\pi}} \int_{-\infty}^{T_s} e^{-(T-T_m)^2 / 2\sigma^2} \, dT$$
(5)

156   where T_s is the rain/snow threshold temperature and T_m is the monthly mean temperature. σ is the

157   standard deviation of daily temperatures.

158   Table 1 Categories of dryness/wetness degree according to the scPDSI values

Categories	scPDSI values
Extremely wet	[4.0, +∞)
Severely wet	[3.0, 4.0)
Moderately wet	[2.0, 3.0)
Mid wet	[1.0, 2.0)
Incipient wet	[0.5, 1.0)
Normal	(-0.5, 0.5)

Incipient dry	(-1.0, -0.5]
Mid dry	(-2.0, -1.0]
Moderately dry	(-3.0, -2.0]
Severely dry	(-4.0, -3.0]
Extremely dry	(-∞, -4.0]

159   To analyse the key global climatic drivers of drought events over Japan, the following four

160   global climatic indices were investigated. The Arctic Oscillation Index (AOI) (Li et al., 2003) and

161   North Atlantic Oscillation Index (NAOI) (Li et al., 2003) are employed to describe the abnormal

162   conditions of the AO and NAO, respectively. These indices are sourced from

163   https://ljp.gcess.cn/dct/page/1 (last access: 10 March 2020). The Pacific Decadal Oscillation Index

164   (PDOI) (Mantua et al., 2002) and Oceanic Niño Index (ONI) (Bamston et al., 1997) respond to the

165   abnormalities of PDO and ENSO, which are sourced from https://www.esrl.noaa.gov/psd/(last access:

166   10 March 2020).

167   **2.3 Trend-Free Pre-whitening Mann-Kendall test**

168   The Mann-Kendall (MK) test, which was proposed by Mann (Mann, 1945) and modified by

169   Kendall (Giglio et al., 2015), is widely used for analysing the change trends in hydrometeorological

170   time series (Liu et al., 2015; Yue et al., 2003a, 2003b). The advantage of the MK test is that the time

171   series does not require any special form for the probability distribution function, which means it is

172   less sensitive to potential interference from outliers in the data (Serrano et al., 1999). However, this

173   test requires that the data should be independent. Some hydrometeorological time series may usually

174   display serial correlation. This will increase the probability that the MK test detects a significant

175   trend, altering the magnitude estimate of serial correlation (Yue et al., 2002). To efficiently eliminate

176   the effect of the serial correlation on the MK trend test, Yue et al. (2002) proposed the trend-free

177   pre-whitening MK (TFPW-MK) test. Before the MK test, the time series is first detrended and

178   pre-whitened. In this paper, we adopted TFPW-MK to analyse the time series trends. The specific

179   details of TFPW-MK can be found in Yue et al. (2002). The main steps are listed as follows:

180   Step 1. Using the Theil-Sen approach (Sen, 1968) estimates the slope b of the trend in the time

181   series. If the slope is equal to zero, then it is unnecessary to continue conducting the trend analysis.

182   If the slope differs from zero, then it is assumed to be linear, and the time series are detrended by the

183   following equation:

184
$$X_t' = X_t - T_t = X_t - bt \qquad (6)$$

185   Step 2. The lag-k serial correlation coefficient r_k of the detrended series X_t' is computed using

186   Equation (7), and then, Autoregressive (k) (AR) is removed from X_t' by Equation (8).

187
$$r_k = \frac{\frac{1}{n-k}\sum_{(t=1)}^{(n-k)}[X_t - E(X_t)][X_{(t+k)} - E(X_t)]}{\frac{1}{n}\sum_{(t=1)}^{n}[X_t - E(X_t)]^2} \qquad (7)$$

188
$$Y_t' = X_t' - r_1 X_{(t-1)}' \qquad (8)$$

189   This pre-whitening procedure after detrending the series is referred to as the TFPW procedure.

190   After applying the TFPW procedure, the time series should be independent.

191   Step 3. The identified trend T_t and the residual Y_t' are blended by the following equation:

192
$$Y_t = Y_t' + T_t \qquad (9)$$

193   Step 4. The MK test is applied to the blended series to assess the significance of the trend. We

194   can obtain the statistic Z through the calculation of the TFPW-MK test and measure the degree to

195   which a trend is consistently decreasing or increasing. In the bilateral trend test, if $|Z| > Z_{1-\alpha/2}$ is at a

196   desired confidence level α, the original hypothesis is unacceptable; that is, the time series trend is not

197   statistically significant at the 1-α confidence level. The confidence levels of 0.05 and 0.1 are equal to

198   the Z values of 1.96 and 1.64, respectively. Thus, the trend can be classified according to the Z value

199   (Table 2) (Wang et al., 2014).

200   Table 2 Trend categories according to the Z values

Categories	Z values
Significant increasing trend	[1.96, +∞)
Weak increasing trend	[1.64, 1.96)
No significant increasing trend	[0, 1.64)
No significant decreasing trend	(-1.64, 0)
Weak decreasing trend	(-1.96, -1.64]
Significant decreasing trend	(-∞, -1.96]

2.4 Distinct Empirical Orthogonal Function

The empirical orthogonal function (EOF), which deals with temporal and spatial functions, is used to extract the spatiotemporal modes based on the data variance representations. The EOF was introduced into meteorology and climate research by Lorenz (1956) in the 1950s and has already been widely applied in other fields, such as geoscience and hydrology. The EOF analysis method can decompose the time-varying variable fields into the space function part (EOFs) that does not change with time and the time function part (principal components, PCs) that depends only on time. The distinct EOF (DEOF) analysis was subsequently introduced to overcome problems in the EOF analysis (Dommenget, 2007). In the DEOF, a continuous spectrum of spatial patterns resulting from a stochastic process can be represented by EOF modes, where some spatial structures will be more dominant than others. Based on the isotropic diffusion null hypothesis, the DEOF modes (DEOFs) can be found by rotating the leading DEOF modes, corresponding to the distinguished principal components (DPCs) (Ye et al., 2019b). These DPCs take up a large part of the total variance in all the variables in the original field, which is equivalent to the main information of the original field concentrated on a few main components. The higher the eigenvalues, the more typical the corresponding modes, and the greater the contribution to the total variance. The details about DEOF can be found in Dommenget (2007).

2.5 Wavelet analysis

The continuous wavelet transform (CWT) (Torrence et al., 1998) is widely used for analysing the frequency domain of hydrometeorological time series (Fang et al., 2018; Li et al., 2020). The spectral and temporal features of the time series can be projected onto a time-frequency plane by CWT, where the dominant cycle period and its duration can be identified (Grinsted et al., 2004). The square modulus of the CWT defines the wavelet power spectrum (WPS) (Jiang et al., 2014), which represents the signal energy at a specific scale (period) and time (Asong et al., 2018). In this paper, the time-frequency domain of DPCs was analysed by CWT. The specific calculation process for CWT can be found in Torrence et al. (1998). Notably, the CWT brings about a cone of influence (COI) that delimits a region of the WPS beyond which the edge effects become significant and the power could be suppressed (Torrence et al., 1998).

229   Also, the cross wavelet transform (XWT) (Torrence et al., 1998) and wavelet coherence (WCO)

230   (Torrence et al., 1999) can examine the relationship between the DPCs and the global climatic

231   driving factor. WCO reveals local similarities between two time series and may be found to be a

232   local correlation coefficient in the time-frequency plane; that is, their possible teleconnection can be

233   identified by WCO (Asong et al., 2018). Similar to the CWT, the parts outside of the COI should

234   also be interpreted with caution. The specific XWT and WCO analysis methods can also be found in

235   Torrence et al. (1998;1999).

3. Results and Discussion

3.1 Variation characteristics of meteorological elements

238   To better understand the drought trends in Japan, the variation characteristics of meteorological

239   elements (precipitation, temperature, and potential evapotranspiration) were first analysed by

240   anomaly curves. Figure 1 shows the anomaly curves of precipitation, temperature, and potential

241   evapotranspiration, which reflects the difference between the annual value of meteorological

242   elements and the overall mean over Japan. For precipitation, there was a weak increasing trend.

243   Moreover, the years with the least precipitation were 1978, 1984, and 1994. The annual scale

244   deviations were -414.91 mm, -411.48 mm, and -339.88 mm respectively.

245   For temperature and potential evapotranspiration, it could be interpreted that these two

246   meteorological elements have similar obvious increasing trends, especially after the late 1970s. Most

247   annual values of temperature and potential evapotranspiration were greater than the overall mean

248   after 1990. In particular, most anomaly values of temperature and potential evapotranspiration

249   appeared in 2004 (0.99 °C) and 1994 (2.42 mm), respectively.

250   The trend analysis of three meteorological elements during different seasons from 1960 to 2018

251   was calculated (see Figure 1). Except for summer, precipitation values have shown an increasing

252   trend in the other three seasons, although these trends were not significant. The temperature and

253   potential evapotranspiration showed a consistent trend in different seasons. The increasing trend was

254   most obvious in spring, while the increasing trend in winter was weakest when compared to other

255   seasons.
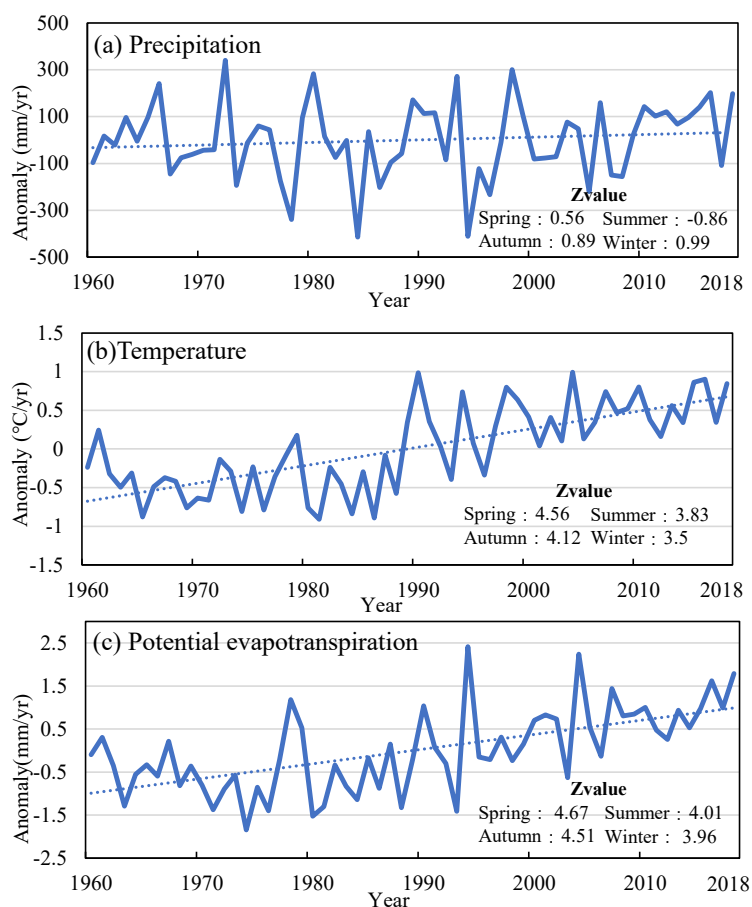
256

257   Figure 1. Average meteorological element anomaly curves and Z value of different seasons over Japan from

258   1960 to 2018. (a) Precipitation. (b) Temperature. (c) Potential evapotranspiration

259   Next, the TFPW-MK trend test results were calculated and then interpolated over Japan by

260   inverse distance weighted (IDW) (see Figure 2). For precipitation, except for some parts of the

261   northernmost region, Japan showed increasing trends. However, all the precipitation trends were

262   insignificant. For temperature, the whole of Japan showed strong increasing trends. The trends in

263   northeast Japan was most significant. For potential evapotranspiration, the trends of potential

264   evapotranspiration were similar to that of temperature. It was evident that almost all of Japan showed

265   increasing trends in potential evapotranspiration, except for several parts of the northernmost region.

266   The trends of potential evapotranspiration in most of eastern Japan were insignificant and only

267   several coastal areas in southwestern Japan showed significant trends. Also, the increased

268   temperature and evapotranspiration could cause the acceleration of soil moisture evaporation loss,

269   which would increase the risk of drought.
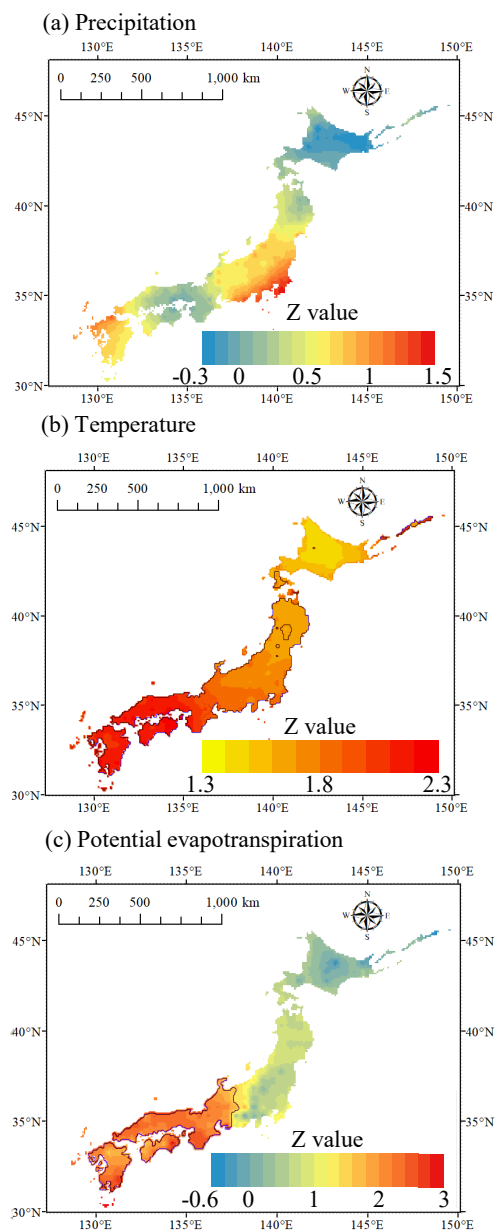
270

271   Figure 2. Meteorological element TFPW-MK trend analysis results over Japan. (The contour indicates that Z value is

272   greater than 1.64) (a) Precipitation. (b) Temperature. (c) Potential evapotranspiration.

273   In addition, in order to reduce the impact of using a single data on the robustness of the results,

274   the trend analysis results of different meteorological elements using different datasets were

275   compared (As shown in the Appendix I). The results showed that the CRU dataset used in this paper

276   was proven to be credible.

277   **3.2 Variation characteristics of drought**

278   For drought, the average scPDSI series of Japan from 1960 to 2018 is shown in Figure 3. A

279   drought month event is defined to occur when the scPDSI is less than -1 (Ye et al., 2019a). The

280   results indicated that the two driest periods occurred in 1983~1988 and 1994~1997. In these two

281   periods, the minimal values of scPDSI were -3.80 and -3.42, which both reached the level of

282   severely dry, as shown in Table 1. To better analyse the size and influence of droughts, the

283   proportions of monthly drought grid points were calculated. The number of grid points where

284   scPDSI ≤-1 is divided by the total number of grid points. These proportions could indirectly reflect

285   the severity of the droughts, as shown in Figure 4. Specifically, there were 193 months out of the 708

286   months from 1960 to 2018 when the drought grid point proportions were ≥50%. In this case, the

287   situation of the drought grid point proportions of ≥90% occurred in 22 months, which meant that

288   drought occurred over almost all of Japan during this several month periods. The range of drought

289   grid point proportions was 0.97 to 0.99 from September 1984 to January 1985 when the maximal

290   value appeared.
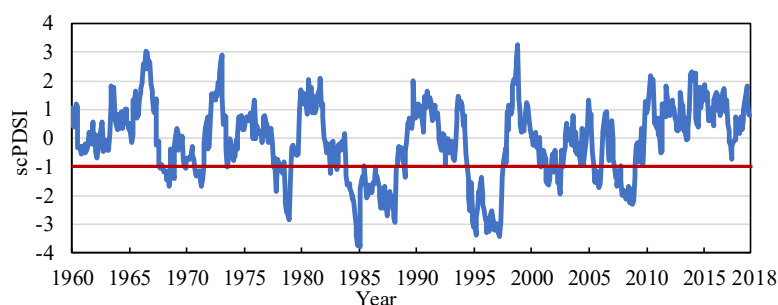
291

292   Figure 3. Average scPDSI time series over Japan from 1960 to 2018. (When scPDSI is less than -1, it means the

293   occurrence of drought month)
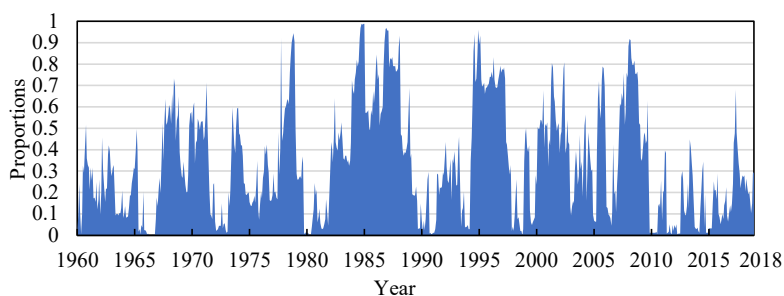
294

295   Figure 4. The drought grid point proportions of the scPDSI over Japan from 1960 to 2018.

296   Also, the number of drought month occurrences in different seasons of each year was counted

297   throughout 1960~2018 (Figure 5). There were 10.1 drought month occurrences on average in 1985

298   with more than two droughts month occurring each season. Indeed, different seasons showed

299   different trends. Figure 6 shows the number of drought month occurrences in different seasons. The

300   percentage of drought month occurrences in spring and summer were observed to be increasing,

301   while the percentage of drought month occurrences in autumn and winter were decreasing. In other

302   words, spring and summer became drier and autumn and winter became wetter in Japan.
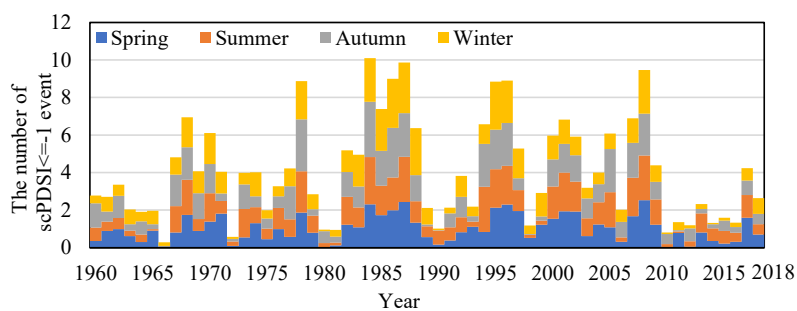
303

304   Figure 5. The number of scPDSI<=-1 event for different seasons over Japan from 1960 to 2018
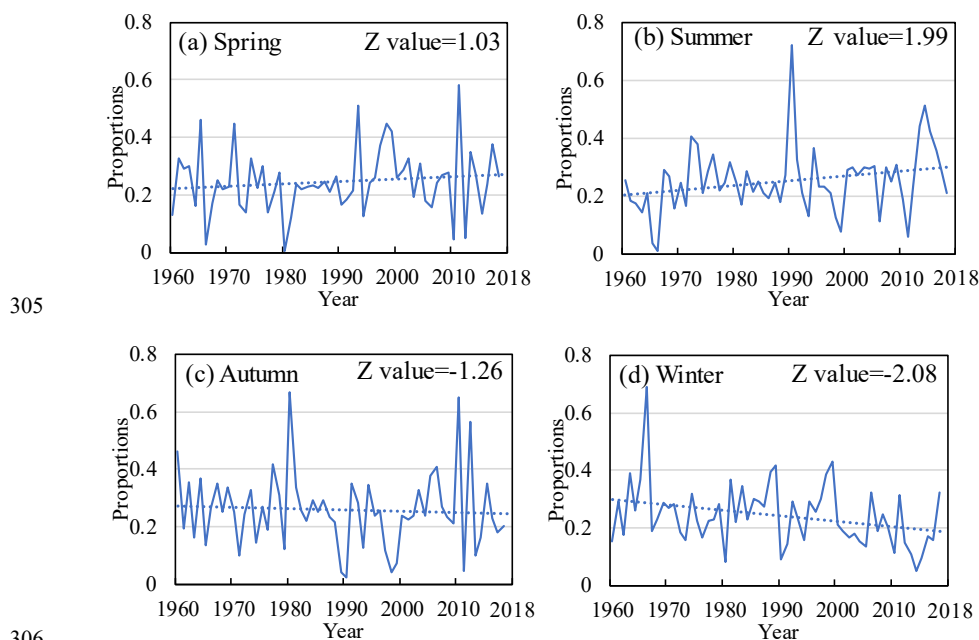
Figure 6. The drought seasonal proportions according to the scPDSI over Japan from 1960 to 2018.

(a) Spring. (b) Summer. (c) Autumn. (d) Winter.

Figure 7a shows the Z values of the scPDSI series at each grid point calculated by the TFPW-MK trend test. Significantly increasing drought trends (decrease in scPDSI) were observed in some western regions. Decreasing trends were found in the northwestern region, the western part of the central region, the partial area of the northeast region, and most of the northernmost region. And when the precipitation and the scPDSI trend analysis results were compared one mesh by one mesh (Figure 7b~c), the trend analysis results of scPDSI varied with the change of precipitation trend.
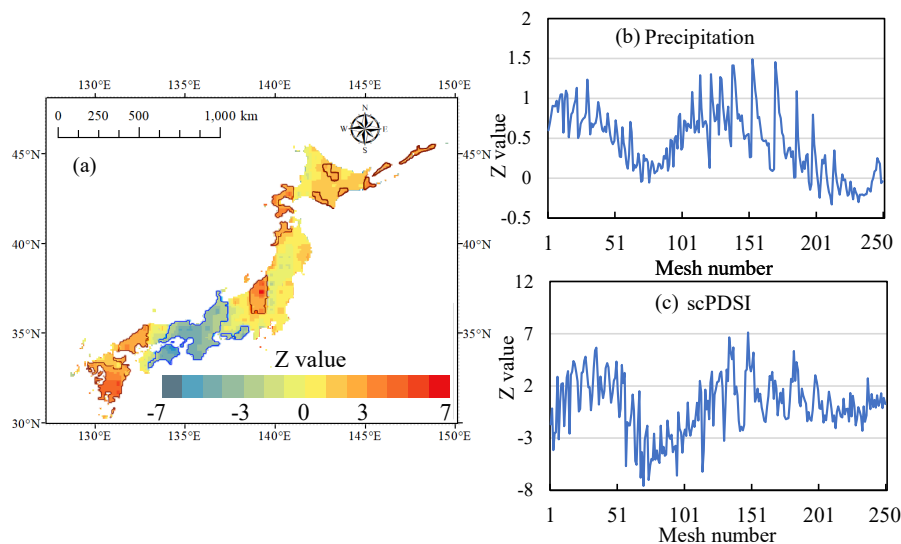
315

316   Figure 7. (a) TFPW-MK trend analysis results over Japan (The blue contour indicates that Z value is less than -1.64;

317   the red contour indicates that Z value is greater than 1.64). (b)~(c) Comparison of the trends of each mesh between

318   precipitation and scPDSI

319   Besides, the comparison of trend analysis results of scPDSI based on different datasets was also

320   applied (As shown in the Appendix II), which proved the robustness of the results.

321 3.3 Spatial and temporal variabilities in drought using DEOF

322   The DEOF calculation used the scPDSI time series of each grid point on the monthly scale.

323   Figure 8a~b displays the spatial partitioning results of the first two DEOFs. The explained variances

324   in the first two DEOFs were 46.85% and 20.55% respectively, which meant that the DEOFs could

325   explain approximately 67.40% of the total spatial wet/dry characteristics of Japan from 1960 to 2018.

326   The first two had sufficiently explained variances to represent most of the wet/dry conditions in

327   Japan. The explained variances in DEOF3 and DEOF4 were only 8.0% and 4.2% respectively. The

328   explained variance in the remaining DEOF values would become much smaller and not considered

329   in this research.

330   The spatial distribution of DEOF1 illustrated that a high positive loading occurred in the

331   western region at approximately 35°N (W region). This finding meant that the W region had similar

332   drought characteristics from 1960 to 2018. Similarly, the spatial distribution of DEOF2 illustrated

333   the common positive spatial behaviour of drought in most of the northernmost region near the

334   Pacific (N region). However, the central region, western region, and most parts of the northwestern

335   region showed common negative spatial behaviour, indicating that these regions showed the opposite

336   drought characteristics as the N region. Notably, the two DEOFs were unable to represent all drought

337   characteristics across the whole of Japan. However, according to their loadings, the whole region

338   could be divided into two drought subregions, the W and N regions, which had different spatial

339   variabilities in drought.

340   For the corresponding drought temporal characteristics, the DPC scores are displayed in Figure

341   9. The DPC1 scores showed a decreasing trend, which meant that the W region became drier.

342   However, the N region was getting wetter. The trends in the DPC scores were consistent with the

343   TFPW-MK trend results in Figure 7. In addition, the drought characteristics in different seasons

344   were analysed. Figures 10~11 show the number and proportion of drought occurrences of DPCs in

345   different seasons. From 1960 to 2018, the number of drought events in the DPC1 scores was highest

346   in spring, accounting for 31%. For the DPC2 scores, the maximal value, 28% of drought occurrences,

347   appeared in autumn.
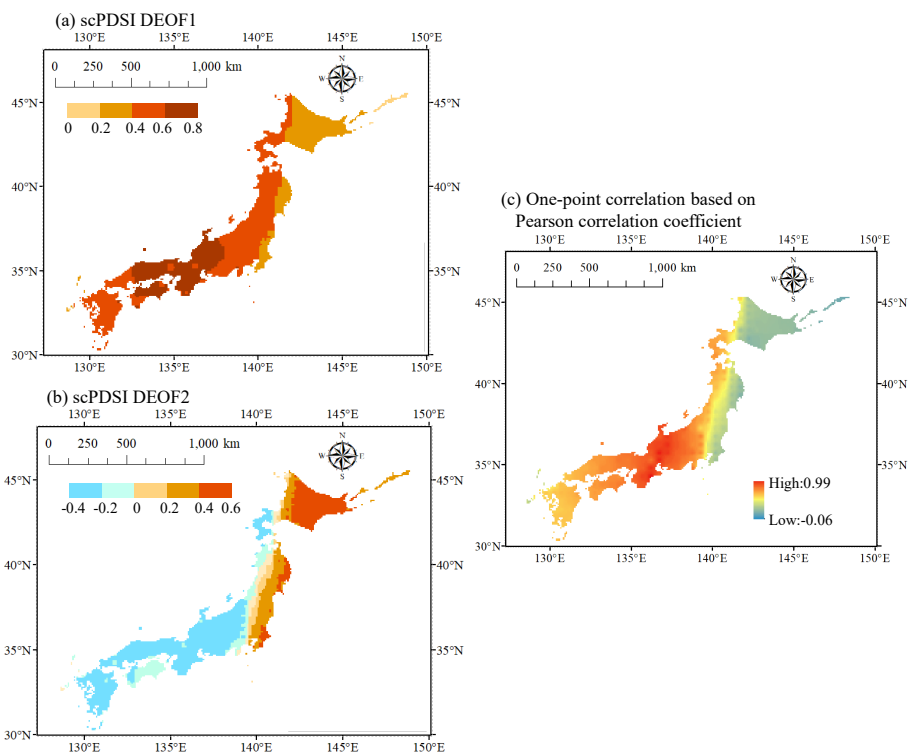
Figure 8. Patterns of the first two DEOFs for scPDSI (a) scPDSI DEOF1. (b) scPDSI DEOF2, and (c) One-point

(34.25°N, 136.25°E) correlation based on Pearson correlation coefficient.
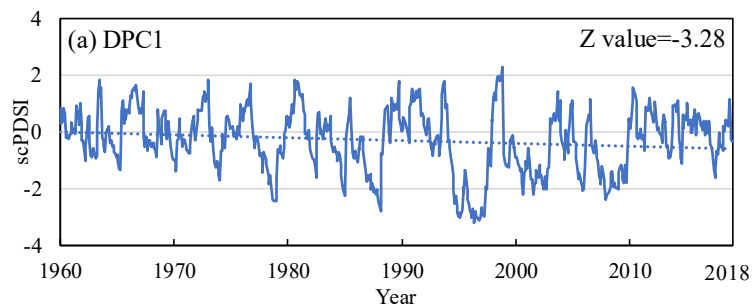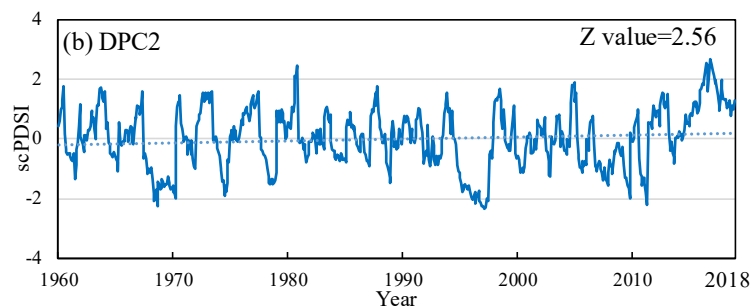
352

353   Figure 9. DPC scores of the first two DEOFs for scPDSI. (a) DPC1. (b) DPC2.
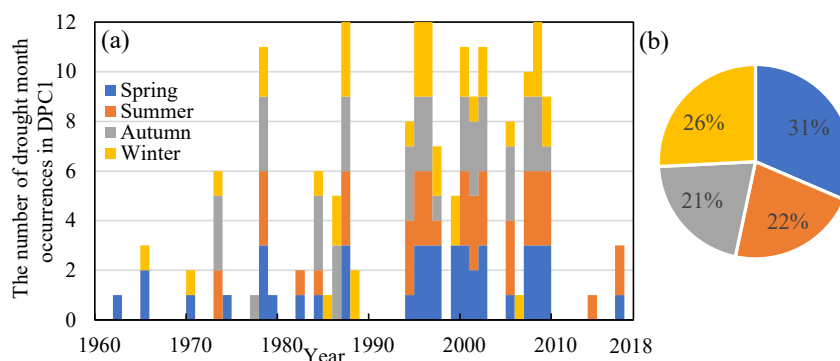
354

355   Figure 10. The number (a) and percentage (b) of drought occurrences in different seasons of DPC1 from 1960 to

356   2018.
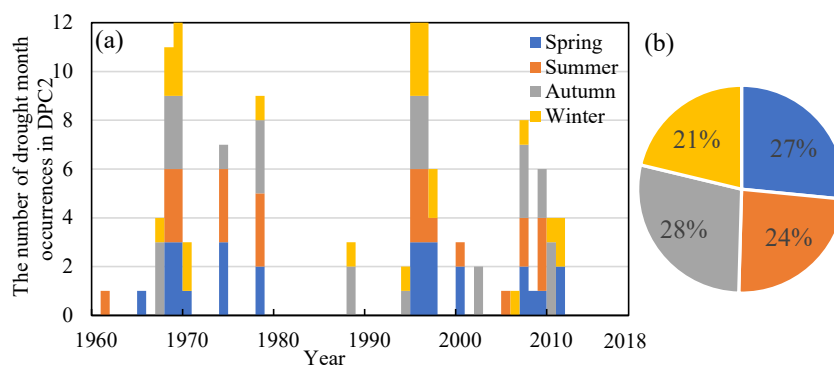
357

358   Figure 11. The number (a) and percentage (b) of drought occurrences in different seasons of the DPC2 from 1960 to

359   2018.

360   **3.4 Comparison between spatial patterns of dryness wildfires**

361   Drought is a factor influencing wildfire occurrence. Considering that drought would cause a

362   decrease in duff moisture and soil moisture, forest fuels (such as grass fallen leaves and branches)

363   become drier and more ignitable, contributing to fire ignition and the subsequent outcomes. Indeed,

364   there have been various studies on the relationship between scPDSI and wildfires. The wildfires in

365   the southern and mountainous ecoregions of the United States showed significant increasing trends,

366   coinciding with trends toward increased drought characterized by scPDSI (Dennison1 et al., 2014).

367   Mongolia experienced a dry period after the 1500s, which coincided with more fires and shorter fire

368   return intervals (Hessl et al., 2016). By comparing various drought indices (PDSI, Drought Index

369   (DI), Monthly Drought Code (MDC), and SPI), the scPDSI was considered to be the best predictor

370   of burned forest area in southern Sweden over 1942-1975 (Drobyshev et al., 2012).

371   Considering the ability of scPDSI to adequately represent the water balance, the analysis of

372   combining drought with wildfires would further enhance the understanding of drought-induced

373   natural disasters. In Japan, the most of wildfires occur in spring, especially in March to May (Suzuki

374   et al., 2009). Therefore, the comparison between the annual burned forest area in spring (March to

375   May) with DPCs was extracted, as shown in Figure 12. The burned area data come from fire reports

376   provided by the Fire and Disaster Management Agency, Government of Japan. The burned area data

377   of the W region included the Ishikawa prefecture, Fukui prefecture, Gifu prefecture, Aichi prefecture,

378   Shiga prefecture, Kyoto prefecture, Osaka prefecture, Hyogo prefecture, Nara prefecture, Wakayama

379   prefecture, Tottori prefecture, Okayama prefecture, and Mie prefecture. The burned area data of the

380   N region included the Hokkaido prefecture.

381   In a wet spring, when the scPDSI was positive, the burned area of western Japan was less than

382   100 ha. The three springs with severe wildfires, when the burned area was larger than 300 ha, were

383   accompanied by drought events in which the scPDSI was less than -1. Although there were fewer

384   wildfire occurrences in the N region than in the W region, these two regions followed a similar

385   pattern. A total of six wildfires with burned areas of over 60 ha occurred in the N region. The scPDSI

386   values corresponding to these six wildfires were all negative, and four of them experienced drought

387   (scPDSI ≤ -1). When the scPDSI was more than 1, there were only six wildfire occurrences in the N

388   region, and the burned area was less than 60 ha.

389 Whether in the W or N region, there was, to a certain extent, a relationship between the wildfire

390 burned area and drought. Indeed, the drought did not necessarily lead to large wildfires, but a lack of

391 soil moisture could increase the risk of severe wildfires. Understanding the effects of drought on

392 other natural disasters could encourage scholars to pay more attention to drought research in Japan.
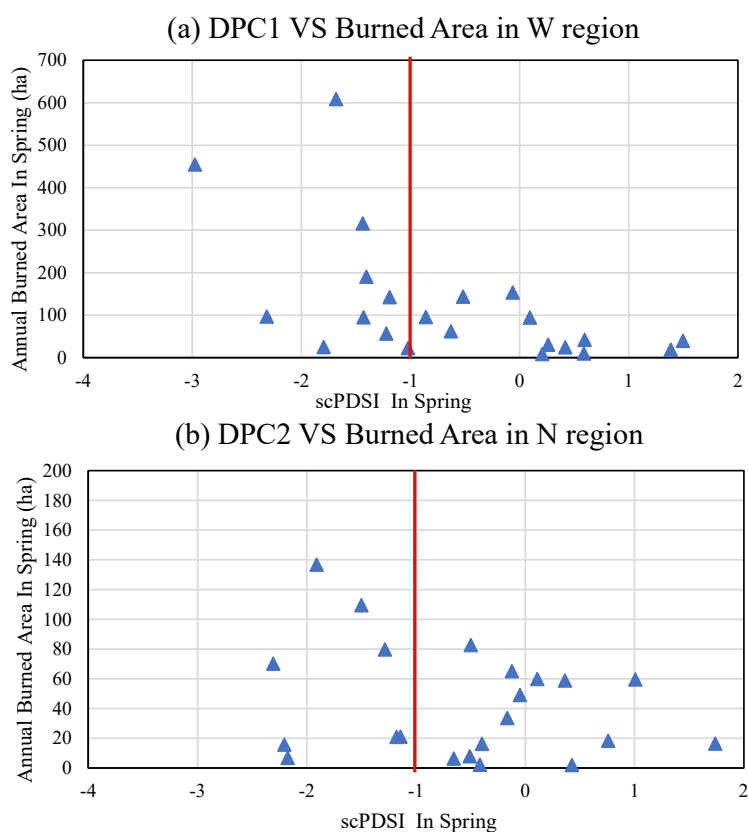
393

394 Figure 12. Comparison of DPCs for annual burned forest area in spring (a) DPC1. (b) DPC2.

395 **3.5 Links between drought and global climatic drivers**

396 Due to the complexity in the causes of drought, the relationship between drought and global

397 climatic drivers needs to be discussed. Figure 13 shows the WPS results of the DPCs of the scPDSI

398 time series. The dominant frequencies of drought were identified. For DPC1 (W region), the

399 significant interannual variability over approximately 44 to 60 months was obvious during the period

400 from 1975 to 1982. Also, a strong dominant frequency band was found to be centred at

401   approximately 48 to 128 months during the mid-1980s to mid-2000s. In the N region (DPC2), a

402   major periodicity of approximately 20 to 56 months was observed in the 1970s. During the 1990s,

403   there was a dominant frequency band of approximately 42 to 58 months. Overall, the frequencies of

404   drought were not strong in DPC1 or DPC2.
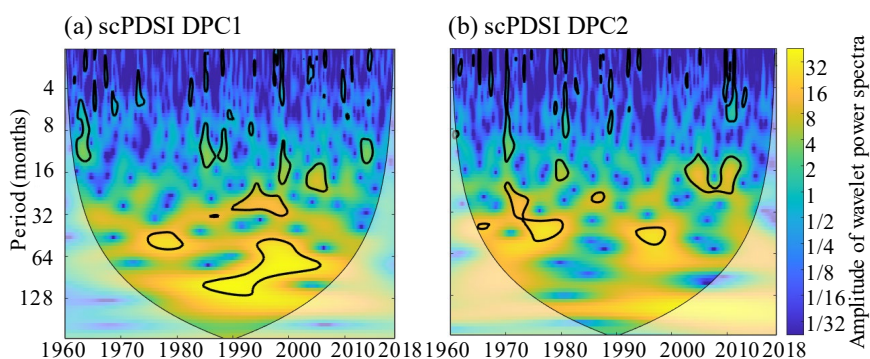
406   Figure 13. WPS of the DPC time series. The black contour designates the 95% confidence level against red noise,

407   and the COI, where edge effects might distort the picture, is shown as a lighter, paler shade.

408   To identify the coherence between drought subregions and climatic causes, the WCO method

409   was used to analyse the covarying occurrence in the dominant frequency bands and time intervals.

410   Figures 14 show the results of the WCO coefficients between the DPCs and climatic driving factors

411   (AOI, NAOI, PDOI, and ONI). In these figures, the level of the coherence and timescale variability

412   between the two time series is represented by different colours corresponding to values that range

413   from 0 to 1. Also, the information inside the thick black lines indicated statistical significance. The

414   arrows illustrate the phase difference between the two time series. If the arrow points to the right

415   (left), then the two time series are in-phase (antiphase). That is, there is a positive correlation

416   (negative correlation). When the arrow points up (down), then the independent variables lead the

417   dependent variables in phase by 3/4 (1/4) of a period. Similarly, if the arrow points to the lower right,

418   lower left, upper right or upper left by 45°, the leading frequency would be 1/8, 3/8, 5/8 or 7/8 of a

419   period, respectively. In this case, because this paper focuses on the impacts of climatic causes on

420   drought, the DPCs were considered to be dependent variables, while the global climatic drivers were

421   considered to be independent variables.

422   For the W region, Figure 14a~b shows that sporadic but significant coherence was found

423   between DPC1 with AOI, NAOI, PDOI, and ONI. For AOI (as shown in Figure 14a), a positive

424   correlation occurred between approximately 96 and 128 months from the 1970s to the mid-1990s,

425   while a temporary negative correlation was found during 1992~2000 in the range of 20 to 32 months.

426   The coherence between DPC1 and NAOI is shown in Figure 14b. It was obvious that the NAOI led

427   the DPC1 in phase by approximately 84 to 112 months from the 1980s to 2000s. However, over the

428   1995~2010 period, DPC1 lagged the NAOI, ranging from 36 to 72 months. In Figure 14c, the

429   directions of the arrows were somewhat messy, meaning that the coherence between PDOI and

430   DPC1 was slightly difficult to determine. But a relatively obvious relationship was that DPC1 lagged

431   PDOI by approximately 8 to 16 months from 1992 to 2005. Also, three strong coherence bands were

432   observed in Figure 14d, one of which was nearly a positive correlation between the DPC1 and ONI

433   in the 1970s. And the ONI led the DPC1 by approximately 12 to 16 months in the 1998~2010 period.

434   From 1998 to 2000, the coherence band was mainly concentrated over 140~168 months.

435   The coherence was stronger in DPC2 than in DPC1. As shown in Figure 14e, a band of

436   approximately 112~128 months of high energy was observed during the period of the mid-1970s to

437   mid-2000s, while the regions beyond the COI were ignored due to edge effects. In this period, the

438   coherence was initially unstable, but after 1985, the relationship between the DPC2 and AOI

439   gradually showed positive correlations. The NAOI (Figure 14f) led the DPC2 by 63~105 months and

440   84~168 months over the periods of 1970~1980 and 1980~2005, respectively. In Figure 14g, from

441   1992 to 2002, the PDOI led the DPC2 by 8 to 16 months, which was similar to the relationship

442   between PDOI and DPC2 during the same period. Besides, the leading relationship of

443   time-frequency became 14~20 months between 2002 and 2010. The correlation between ONI and

444   drought was relatively weak compared with the other three climatic factors. The results indicated

445   that the ONI (Figure 14h) led the DPC2 by 14~18 months from 1995 to 2010.
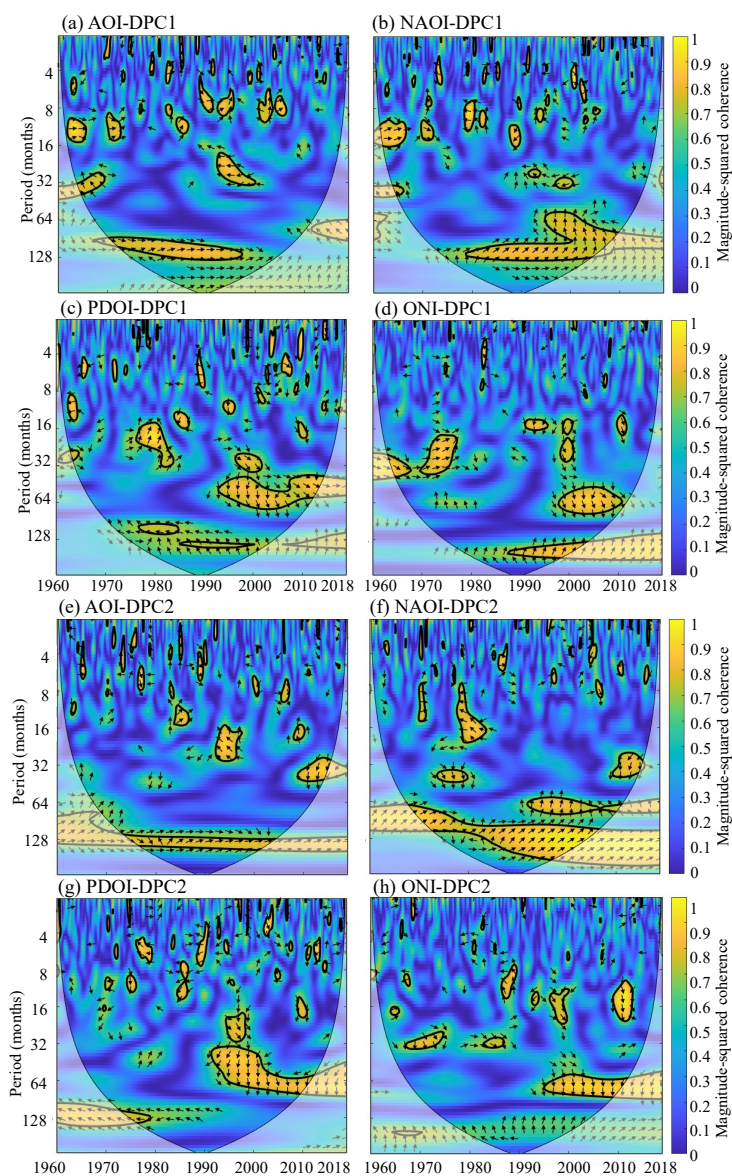
Figure 14. Squared wavelet coherence between the global climatic driving factors and the temporal patterns in the W region and N region. (a) AOI-DPC1. (b) NAOI-DPC1. (c) PDOI-DPC1. (d) ONI-DPC1 (e) AOI-DPC2. (f) NAOI-DPC2. (g) PDOI-DPC2. (h) ONI-DPC2. The black contour designates the 95% confidence level against red noise, and the COI, where edge effects might distort the picture, is shown as a lighter, paler shade

451   The foregoing analysis has shown the teleconnection between drought over Japan and global

452   climatic drivers. This paper mainly focused on qualitative analyses to determine the climatic driving

453   factors that have the most obvious impact on drought rather than focusing on quantitative analyses.

454   For DPC1, the most significant coherence between DPC1 and NAOI occurred from the 1980s to

455   2000s, and the dominant frequency of DPC1 appeared in 1985~2005, which suggested that the

456   periodic features of drought in the W region were likely to be affected by the NAO. For the N region,

457   the significant coherence between drought with the AO and NAO appeared throughout the research

458   period, but because of the edge effects, the coherence analysis mainly revolves around the parts in

459   the COI. This finding also showed that the complexity in the cause of the drought was affected by

460   more than one climatic driving factor. The CWT and WTC analysed the relationship between

461   drought and global climatic driving factors from only a statistical point of view, so the underlying

462   physical process was not the target of this research. However, this paper would be meaningful for

463   determining the climatic driving factors that affect the occurrence of drought, and in-depth research

464   on predicting droughts through climatic driving factors is required.

465   Additionally, this paper identified the two global climatic drivers, AO and NAO, which had the

466   most significant effects on drought over Japan. But the effects of these two global climatic drivers on

467   regional climate is not limited to Japan. Actually, in the Korean Peninsula across the sea from Japan,

468   the spring drought events in this region have also been confirmed to be affected by the NAO (Kim et

469   al., 2017). Also, the majority of UK recorded droughts in recent history showed a clear relationship

470   with NAO (Rust et al., 2019). Even in the northeastern United States, drought prediction was

471   performed based on NAO (Berton et al., 2017). The AO had significantly affected the extreme

472   drought event over southwestern China (Yang et al., 2012), hydrological drought over Turkey and

473   northern Iran (Vazifehkhah et al., 2018), and climatological drought over Finland (Irannezhad et al.,

474   2017). Global climatic drivers such as NAO and AO had vast and far-reaching effects on the

475   different regional hydroclimate. This paper is the first to connect the drought over Japan with NAO

476   and AO. The discovery of regional droughts with similar climatic causes would also provide the

477   basis for conducting further research on different drought teleconnection analysis in different

478   regions.

4. Summary and Conclusions

479

480   Investigation of the coherence connections between drought and global climatic driving factors

481 is significant for a better understanding of drought. This paper focused on Japan, which has less

482 available drought-related research, as the research area and provided a comprehensive analysis of

483 drought patterns over Japan during the period from 1960 to 2018 using the scPDSI drought index.

484 The relationship between wildfire burned area and the scPDSI was analysed. Wavelet analysis was

485 applied to detect the climatic driving factors that had the strongest relationship with drought, which

486 overcame the insufficiency of classical drought analysis in determining the cause of the drought.

487   The main conclusions obtained from this paper are summarized as follows: (1) The potential

488 evapotranspiration and temperature showed increasing trends throughout almost all of Japan, while

489 the changing trend in precipitation was not significant. The changes in potential evapotranspiration

490 and precipitation were most obvious in summer, whereas there was little difference in the

491 temperature in different seasons. (2) On average, 1983~1988 and 1994~1997 were the two driest

492 periods in Japan. Also, the droughts were greater in spring and summer and weaker in autumn and

493 winter. (3) DEOF was used to identify two major subregions of drought variability—the western

494 region (W region) and most of the northernmost region near the Pacific (N region). The

495 corresponding scores of DPC1 and DPC2 showed a trend of decreasing (increasing in drought) and

496 increasing (decreasing in drought), respectively. (4) When scPDSI was less than -1, wildfires with

497 larger burned areas were more likely to occur. (5) The global climatic driving factors that showed the

498 strongest cross-correlation with DPC1 and DPC2 were the NAOI and AOI together with the NAOI,

499 respectively, and their corresponding coherence times were 1980~2010 and 1975~2005, respectively.

500   The outputs of the paper provide a reference for the future study of drought prediction in Japan.

501 Through the identification of drought subregions with similar drought spatiotemporal characteristics,

502 it can be helpful for drought risk management at the regional scale over Japan. The analysis of the

503 climatic causes of drought in these subregions can be useful for choosing suitable impact factors for

504 drought predictions.

5. Appendices

505

506 **Appendix I:** To analyze the robustness of trend results, the precipitation and temperature data from

507 the Automated Meteorological Data Acquisition System (AMeDAS) of Japan Meteorological

508 Agency and the radiation, wind speed and dew point temperature from Dynamical Regional

509 Downscaling Using Japanese 55-year Reanalysis Data (DSJRA55)(Kayaba et al., 2016) were

510 selected. Due to the time scale of DSJRA55 data is only available from 1958~2012, this paper only

511 compared the consistency of the data from 1958 to 2012. The specific results are shown in the Figure

512 A1~A3. Although the results of the two datasets were a little different, the trend analysis results

513 in most areas were consistent.
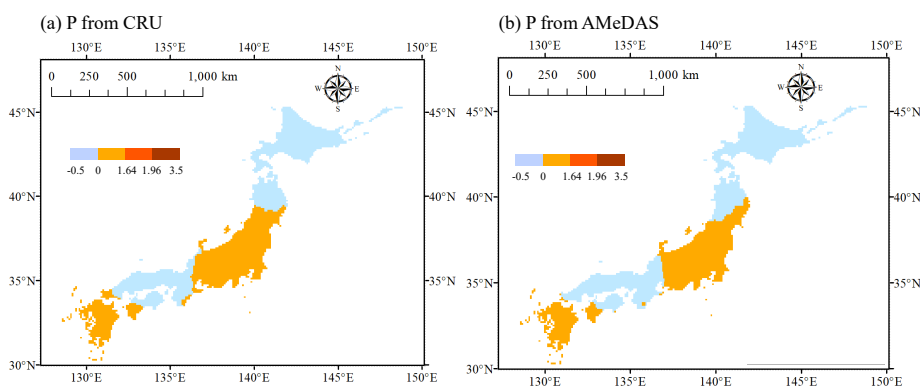
515 Figure A1. TFPW-MK trend analysis results of precipitation based on different datasets from 1960~2012

516 (Display of Significant area).
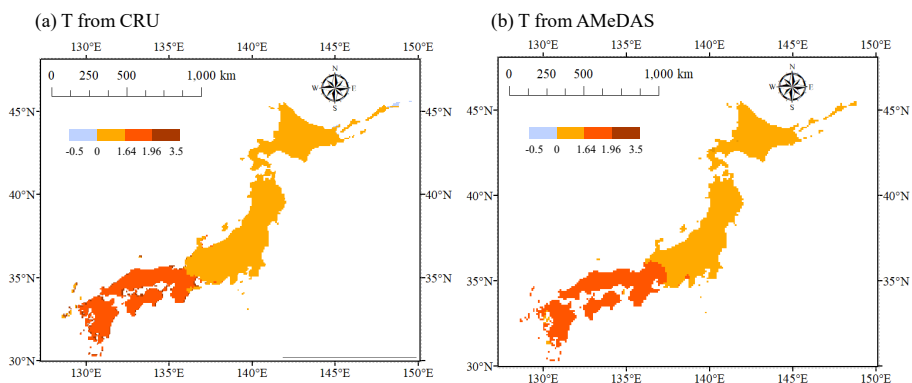
518 Figure A2. TFPW-MK trend analysis results of temperature based on different datasets from 1960~2012

519 (Display of Significant area).
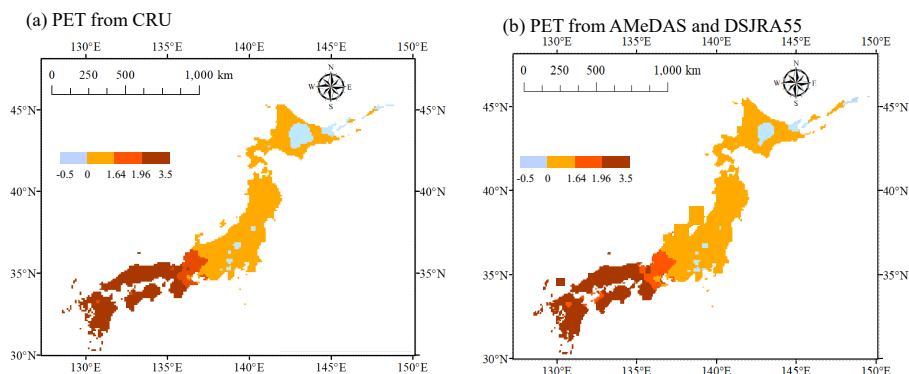
520

521   Figure A3. TFPW-MK trend analysis results of potential evapotranspiration based on different datasets from

522   1960~2012 (Display of Significant area).

523   **Appendix II:** Based on the data mentioned in Appendix I, the scPDSI based on the different datasets

524   were also compared during the period of 1958~2012 (As shown in Figure A4).

525
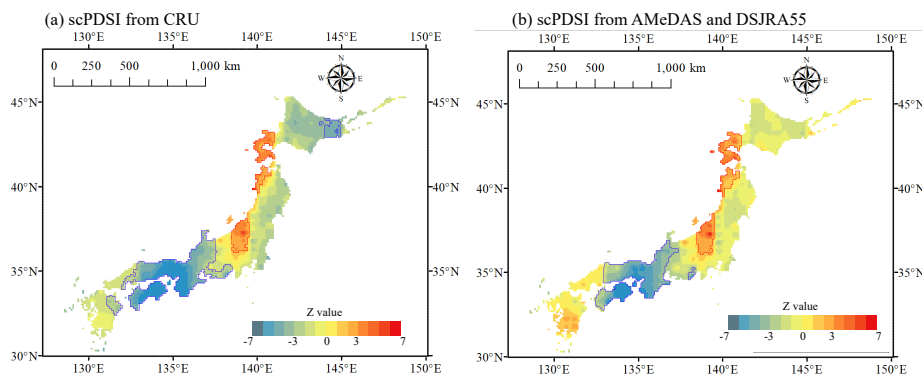
526

527

528   Figure A4. Trend analysis results of scPDSI based on different datasets from 1960~2012. (The blue contour

529   indicates that Z value is less than -1.64; the red contour indicates that Z value is greater than 1.64)

530   **Data availability**

531   All datasets utilized to perform this study are freely available on the internet. For further

532   information, please contact the corresponding author.

533   **Author contributions**

534   **Ke Shi:** Methodology, Software, Formal analysis, Original Draft; **Yoshiya Touge:** Data

535   Curation, Review & Editing, Project administration, Funding acquisition. **So Kazama:** Supervision,

536   Project administration, Funding acquisition.

537   **Competing Interest**

538   The authors declare no conflicts of interest.

539   **Acknowledgements**

540   Yoshiya Touge and So Kazama are supported by the Japan Society for the Promotion of

541   Science.

542   **Financial support**

543   This research was partially supported by the Grant-in Aid for Scientific Research (B),

544   2020-2023 (20H02248, Yoshiya Touge) and Ministry of Education, Science, Sports and Culture,

545   Grant-in-Aid for Exploratory Research, 2019-2021 (19K21982, So Kazama).

546   # References

547   Aizen, E. M., Aizen, V. B., Melack, J. M., Nakamura, T. and Ohta, T.: Precipitation and

548   atmospheric circulation patterns at mid-latitudes of Asia, Int. J. Climatol., 556, 535–556, 2001.

549   Allen, R. G. and Pereira, L. S.: Crop evapotranspiration - Guidelines for computing crop water

550   requirements - FAO Irrigation and drainage paper 56., 1998.

551   Asong, Z. E., Wheater, H. S., Bonsal, B., Razavi, S. and Kurkute, S.: Historical drought patterns

552   over Canada and their teleconnections with large-scale climate signals, Hydrol. Earth Syst. Sci.,

553   22(6), 3105–3124, 2018.

554   Bamston, A. G., Chelliah, M. and Goldenberg, S. B.: Documentation of a highly enso-related sst

555   region in the equatorial pacific: Research note, Atmos. - Ocean, 35(3), 367–383, 1997.

556   Berton, R., Driscoll, C. T. and Adamowski, J. F.: The near-term prediction of drought and

557   flooding conditions in the northeastern United States based on extreme phases of AMO and

558   NAO, J. Hydrol., 553, 130–141, 2017.

559   Blunden, J., Arndt, D. S. and Hartfield, G.: State of the climate in 2017, Spec. Suppl. to Bull.

560   Am. Meteorol. Soc., 99(8), 129–150, 2019.

561   Chuvieco, E., Pettinari, M. L., Lizundia-Loiola, J., Storm, T. and Padilla Parellada, M.: ESA

562   Fire Climate Change Initiative (Fire_cci): MODIS Fire_cci Burned Area Pixel product, version

563   5.1[dataset], Cent. Environ. Data Anal., 2018.

564   Cook, E. R., Woodhouse, C. A., Eakin, C. M., Meko, D. H. and Stahle, D. W.: Long-term aridity

565   changes in the western United States, Science., 306(5698), 1015–1018, 2004.

566   Dai, A.: Drought under global warming: A review, Wiley Interdiscip. Rev. Clim. Chang., 2(1),

567   45–65, 2011.

568   Dai, A.: Increasing drought under global warming in observations and models, Nat. Clim.

569   Chang., 3(1), 52–58, 2013.

570   Dennison, P. E., Brewer, S. C., Arnold, J. D. and Moritz, M. A.: Large wildfire trends in the

571   western United States, 1984–2011, Geophys. Res. Lett., 10(1002), 2928–2933, 2014.

572   Dommenget, D.: Evaluating EOF modes against a stochastic null hypothesis, Clim. Dyn., 28(5),

573   517–531, 2007.

574   Drobyshev, I., Niklasson, M. and Linderholm, H. W.: Forest fire activity in Sweden: Climatic

575   controls and geographical patterns in 20th century, Agric. For. Meteorol., 154–155, 174, 2012.

576   Edwards, B., Gray, M. and Hunter, B.: The social and economic impacts of drought, Aust. J. Soc.

577   Issues, 54(1), 22–31, 2019.

578   Fang, Y., Qian, H., Chen, J. and Xu, H.: Characteristics of spatial-temporal evolution of

579   meteorological drought in the Ningxia Hui autonomous region of northwest China, Water

580   (Switzerland), 10(8), 2018.

581   Giglio, L., Justice, C., Boschetti, L. and Roy, D.: MCD64A1 MODIS/Terra+Aqua Burned Area

582   Monthly L3 Global 500m SIN Grid V006 [Data set], Elsevier B.V., 2015.

583   Grinsted, A., Moore, J. C. and Jevrejeva, S.: Application of the cross wavelet transform and

584   wavelet coherence to geophysical time series, Nonlinear Process. Geophys., 11(5/6), 561–566,

585   2004.

586   Hagman, G.: Prevention Better than Cure: Report on Human and Natural Disasters in the Third

587   World., 1984.

588   Harris, I., Jones, P. D., Osborn, T. J. and Lister, D. H.: Updated high-resolution grids of monthly

589   climatic observations - the CRU TS3.10 Dataset, Int. J. Climatol., 34(3), 623–642, 2014.

590   He, S., Gao, Y., Li, F., Wang, H. and He, Y.: Impact of Arctic Oscillation on the East Asian

591   climate: A review, Earth-Science Rev., 164, 48–62, 2017.

592   Hessl, A. E., Brown, P., Byambasuren, O., Cockrell, S., Leland, C., Cook, E., Nachin, B.,

593   Pederson, N., Saladyga, T. and Suran, B.: Fire and climate in Mongolia (1532–2010 Common

594   Era), Geophys. Res. Lett., 43(12), 6519–6527, 2016.

595   Hisdal, H.: Drought Event Definition., 2000.

596   Hu, Z. Z., Wu, R., Kinter, J. L. and Yang, S.: Connection of summer rainfall variations in South

597   and East Asia: Role of El Niño-southern oscillation, Int. J. Climatol., 25(9), 1279–1289, 2005.

598   Iglesias, A., Garrote, L., Flores, F. and Moneo, M.: Challenges to manage the risk of water

599   scarcity and climate change in the Mediterranean, Water Resour. Manag., 21(5), 775–788, 2007.

600   IPCC: Climate Change 2014 Part A: Global and Sectoral Aspects., 2014.

601   Irannezhad, M., Ahmadi, B., Kløve, B. and Moradkhani, H.: Atmospheric circulation patterns

602   explaining climatological drought dynamics in the boreal environment of Finland, 1962–2011,

603   Int. J. Climatol., 37(March), 801–817, 2017.

604   Jiang, R., Gan, T. Y., Xie, J. and Wang, N.: Spatiotemporal variability of Alberta's seasonal

605   precipitation, their teleconnection with large-scale climate anomalies and sea surface

606   temperature, Int. J. Climatol., 34(9), 2899–2917, 2014.

607   Kayaba, N., Yamada, T., Hayashi, S., Onogi, K., Kobayashi, S., Yoshimoto, K., Kamiguchi, K.

608   and Yamashita, K.: Dynamical regional downscaling using the JRA-55 reanalysis (DSJRA-55),

609   Sci. Online Lett. Atmos., 12(1), 1–5, 2016.

610   Kim, J. S., Seo, G. S., Jang, H. W. and Lee, J. H.: Correlation analysis between Korean spring

611   drought and large-scale teleconnection patterns for drought forecasting, KSCE J. Civ. Eng.,

612   21(1), 458–466, 2017.

613   Kogan, F. and Guo, W.: Early twenty-first-century droughts during the warmest climate,

614   Geomatics, Nat. Hazards Risk, 7(1), 127–137, 2016.

615   Lee, M. H., Ho, C. H., Kim, J. H. and Song, H. J.: Low-frequency variability of tropical

616   cyclone-induced heavy rainfall over East Asia associated with tropical and North Pacific sea

617   surface temperatures, J. Geophys. Res. Atmos., 117(12), 1–11, 2012a.

618   Lee, S. M., Byun, H. R. and Tanaka, H. L.: Spatiotemporal Characteristics of Drought

619   Occurrences over Japan, J. Appl. Meteorol. Climatol., 51(6), 1087–1098, 2012b.

620   Li, J. and Wang, J. X. L.: A new North Atlantic Oscillation index and its variability, Adv. Atmos.

621   Sci., 20(5), 661–676, 2003.

622   Li, Q., He, P., He, Y., Han, X., Zeng, T., Lu, G. and Wang, H.: Investigation to the relation

623   between meteorological drought and hydrological drought in the upper Shaying River Basin

624   using wavelet analysis, Atmos. Res., 234(March 2019), 104743, 2020.

625   Liu, X., Wang, S., Zhou, Y., Wang, F., Li, W. and Liu, W.: Regionalization and Spatiotemporal

626   Variation of Drought in China Based on Standardized Precipitation Evapotranspiration Index

627   (1961-2013), Adv. Meteorol., 2015, 2015.

628   Lorenz, E. N.: Empirical Orthogonal Functions and Statistical Weather Prediction, Tech. Rep.

629   Stat. Forecast Proj. Rep. 1 Dep. Meteorol. MIT 49, 1(Scientific Report No. 1, Statistical

630   Forecasting Project), 52, 1956.

631   Mann, H. B. .: Nonparametric Tests Against Trend, Econometrica, 13(3), 245–259, 1945.

632   Mantua Nathan J. and Hare Steven R.: The pacific decadal oscillation, J. Oceanogr., 58(Figure

633   23), 35–44, 2002.

634   Mishra, A. K. and Singh, V. P.: A review of drought concepts, J. Hydrol., 391(1–2), 202–216,

635   2010.

636   MLIT: Water in Japan., 2014.

637   Okada, T.: Integrated water resources management and drought risk management in Japan,

638   Water Policy, 18, 70–88, 2016.

639   Palmer, W. C.: Meteorological Drought., 1986.

640   Rajagopalan, B., Cook, E., Lall, U. and Ray, B. K.: Spatiotemporal variability of ENSO and

641   SST teleconnections to summer drought over the United States during the twentieth century, J.

642   Clim., 13(24), 4244–4255, 2000.

643   Rangsiwanichpong, P., Kazama, S. and Ekkawatpanit, C.: Analysing the relationship between

644   ocean indices and rainfall in the Chao Phraya River Basin, Int. J. Climatol., 37(January), 230–

645   238, 2017.

646   Rust, W., Holman, I., Bloomfield, J., Cuthbert, M. and Corstanje, R.: Understanding the

647   potential of climate teleconnections to project future groundwater drought, Hydrol. Earth Syst.

648   Sci., 23(8), 3233–3245, 2019.

649   Sarris, D., Christopoulou, A., Angelonidi, E., Koutsias, N., Fulé, P. Z. and Arianoutsou, M.:

650   Increasing extremes of heat and drought associated with recent severe wildfires in southern

651   Greece, Reg. Environ. Chang., 14(3), 1257–1268, 2014.

652   Van Der Schrier, G., Barichivich, J., Briffa, K. R. and Jones, P. D.: A scPDSI-based global data

653   set of dry and wet spells for 1901-2009, J. Geophys. Res. Atmos., 118(10), 4025–4048, 2013.

654   Sen, P. K.: Estimates of the Regression Coefficient Based on Kendall's Tau, J. Am. Stat. Assoc.,

655   63(324), 1379–1389, 1968.

656   Serrano, A., Mateos, V. L. and García, J. A.: Trend analysis of monthly precipitation over the

657   Iberian Peninsula for the period 1921-1995, Phys. Chem. Earth, Part B Hydrol. Ocean. Atmos.,

658   24(1–2), 85–90, 1999.

659   Sheffield, J., Andreadis, K. M., Wood, E. F. and Lettenmaier, D. P.: Global and continental

660   drought in the second half of the twentieth century: Severity-area-duration analysis and

661   temporal variability of large-scale events, J. Clim., 22(8), 1962–1981, 2009.

662   Su, Y., Gao, W. and Guan, D.: Integrated assessment and scenarios simulation of water security

663   system in Japan, Sci. Total Environ., 671, 1269–1281, 2019.

664   Suzuki, S., Yoshitakei, T. and Goto, Y.: Values for forest damage caused by strong wind, heavy

665   rain, snow and forest fire based on statistics compiled in Japan from fiscal year 1954 to 2003,

666   Bull. FFPRI, 8(1), 71–100, 2009.

667   Torrence, C. and Compo, G. P.: A Practical Guide to Wavelet Analysis, Bull. Am. Meteorol. Soc.,

668   79(1), 61–78, 1998.

669   Torrence, C. and Webster, P. J.: Interdecadal changes in the ENSO-monsoon system, J. Clim.,

670   12(8 PART 2), 2679–2690, 1999.

671   Vazifehkhah, S. and Kahya, E.: Hydrological drought associations with extreme phases of the

672   North Atlantic and Arctic Oscillations over Turkey and northern Iran, Int. J. Climatol., 38(12),

673   4459–4475, 2018.

674   Viste, E., Korecha, D. and Sorteberg, A.: Recent drought and precipitation tendencies in

675   Ethiopia, Theor. Appl. Climatol., 112(3–4), 535–551, 2013.

676   Wang, F., Yamamoto, H. and Ibaraki, Y.: Responses of some landscape trees to the drought and

677   high temperature events during 2006 and 2007 in Yamaguchi, Japan, J. For. Res., 20(3), 254–

678   260, 2009.

679   Wang, W., Zhu, Y., Xu, R. and Liu, J.: Drought severity change in China during 1961–2012

680   indicated by SPI and SPEI, Nat. Hazards, 75(3), 2437–2451, 2014.

681   Wells, N. and Goddard, S.: A Self-Calibrating Palmer Drought Severity Index, J. Clim., 17,

682   2335–2351, 2004.

683   Wilhite, D. A., Svoboda, M. D. and Hayes, M. J.: Understanding the complex impacts of

684   drought: A key to enhancing drought mitigation and preparedness, Water Resour. Manag., 21(5),

685   763–774, 2007.

686   Yang, J., Gong, D., Wang, W., Hu, M. and Mao, R.: Extreme drought event of 2009/2010 over

687   southwestern China, Meteorol. Atmos. Phys., 115(3–4), 173–184, 2012.

688   Ye, L., Shi, K., Xin, Z., Wang, C. and Zhang, C.: Compound droughts and heat waves in China,

689   Sustain., 11(12), 2019a.

690   Ye, L., Shi, K., Zhang, H., Xin, Z., Hu, J. and Zhang, C.: Spatio-temporal analysis of drought

691   indicated by SPEI over Northeastern China, Water (Switzerland), 11(5), 2019b.

692   Yue, S. and Hashino, M.: Long term trends of annual and monthly precipitation in Japan, J. Am.

693   Water Resour. Assoc., 39(3), 587–596, 2003a.

694   Yue, S. and Hashino, M.: Temperature trends in Japan: 1900-1996, Theor. Appl. Climatol.,

695   75(1–2), 15–27, 2003b.

696   Yue, S. and Wang, C.: Applicability of prewhitening to eliminate the influence of serial

697   correlation on the Mann-Kendall test, Water Resour. Res., 38(6), 1–7, 2002.

698   Yue, S., Pilon, P., Phinney, B. and Cavadias, G.: The influence of autocorrelation on the ability

699   to detect trend in hydrological series, Hydrol. Process., 16(9), 1807–1829, 2002.

700